Natural carbonation boost for hardened cement fines by dripping technique

Dayoung Oh[a], Ryoma Kitagaki[a*], Takayoshi Masuo[b], Zhijiang Li[a], Ryo Kurihara[c], Takafumi Noguchi[c], Ippei Maruyama[c,d]

[a]*Graduate School of Engineering, Hokkaido University, Nishi-8-chome, Kita-13-jyo, Kita-ku, Sapporo-shi, Hokkaido 060-8628, Japan*

[b]*Masuo Recycle Co.,Ltd, 18-1, Nishinippori 2-chome, Arakawa-ku, Tokyo, 116-0013, Japan*

[c]*Department of Architecture, The University of Tokyo, 7-3-1, Hongo, Bunkyo-ku, Tokyo 113-8685, Japan*

[d]*Department of Environmental Engineering and Architecture, Nagoya University, Nagoya 464-8603, Japan*

[*]Corresponding author. Tel.: +81-11-706-6239; fax: +81-11-706-6240.

E-mail address: ryoma@eng.hokudai.ac.jp (R. Kitagaki).

Graphical Abstract

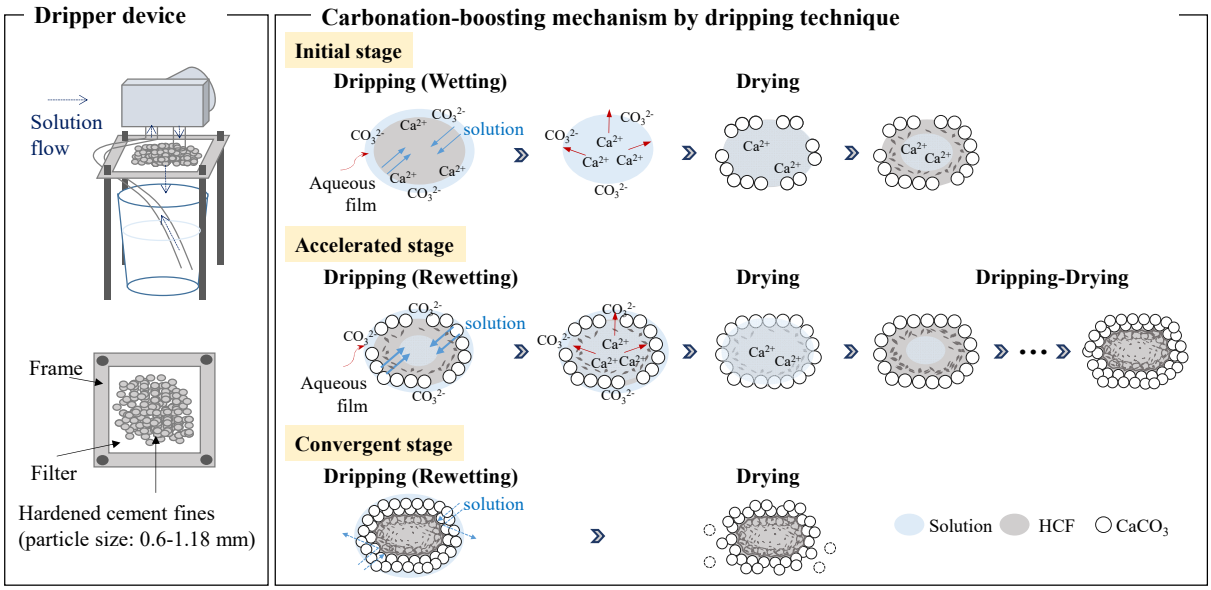

Abstract

This study proposes a dripping technique to improve the carbonation efficiency of hardened cement fine (HCF), which mimicked the binder part of waste concrete, sized between 0.6 mm to 1.18 mm under atmospheric CO_2 concentration. After a 7-day carbonation using the dripping technique, the carbonation degree doubled compared with that at 85 % relative humidity (RH). This improved carbonation efficiency can be attributed to two factors: 1) The pores created during drying accelerate the infiltration of the solution, releasing more calcium ions; 2) The difference in calcium ion concentration between the surface aqueous film and pore solution causes calcium ions to migrate to the surface, accelerating the dissolution of calcium-bearing hydrates in the pore solution and releasing more calcium ions. Adjusting the dripping interval and drying conditions according to the particle size and amount of carbonatable calcium improves the carbonation efficiency. This strategic approach offers a practical means to contribute to the sustainable recycling of waste concrete.

Keywords: Drying; Humidity; Thermodynamic Calculations; Carbonation; Cement Paste.

Abbreviations: hardened cement fine (HCF), calcium-silicate-hydrate (C-S-H), thermogravimetric analysis (TGA), powder X-ray diffraction (XRD), Fourier transform infrared spectroscopy in attenuated total reflection mode (FTIR-ATR), Scanning Electronic Microscopy (SEM), isopropanol (IPA).

1. Introduction

In the pursuit of mitigating global warming, research on CO_2 reabsorption utilising waste concrete containing calcium-silicate-hydrate (C-S-H) and calcium hydroxide ($Ca(OH)_2$), which can absorb CO_2, is being actively conducted in the construction and building material field [1-7]. Currently, most waste concrete is recycled as roadbed material. It is typically stored in open yards for approximately one week to one month before being recycled. Proposing a method to maximise CO_2 absorption during this limited timeframe before waste concrete is recycled aligns with the social need to reduce atmospheric CO_2.

The key elements for concrete to absorb CO_2 include carbonate ions, calcium ions, and an environment allowing for the reaction described in Eq. (1).

$$Ca^{2+} + CO_3^{2-} \rightarrow CaCO_3 \qquad (1)$$

A solvent is required to release calcium ions. The main calcium-bearing hydrates in concrete are C-S-H and $Ca(OH)_2$, which dissolve in water and release calcium ions based on their solubility. Therefore, the larger the amount of water, the larger the amount of calcium ions released. Meanwhile, assuming a constant atmospheric CO_2 concentration, CO_2 diffusion into the concrete is necessary for an optimal reaction between CO_2 and the calcium ions dissolved in the concrete pore water. It should be noted that concrete pore water hinders CO_2 diffusion. The diffusion coefficient of CO_2 in air-filled pores at 298 K is 1.65×10^{-5} m^2/s [8]. In water, CO_2 diffusion is slower by four orders of magnitude than in air [9]. Consequently, water releases calcium ions through the dissolution of calcium-bearing hydrates and acts as a reaction medium in which the released ions combine to precipitate carbonates, whereas it hinders CO_2 diffusion during the carbonation process [5,10].

Many studies have reported that intermediate relative humidity (RH) (50-70%) is the most optimal condition for carbonation: although fewer calcium ions are released than at higher RH, CO_2 diffuses more into the particle [11-14]. On the other hand, smaller particles have an increased specific surface area, and the distance to the center of the smaller particle becomes shorter in proportion to the particle size. Therefore, the carbonation is faster at high relative humidity (RH) [2,6,15], where a substantial

amount of calcium ions is released from the surface, because the mass transfer from the surface to the center is negligible. Therefore, particle size significantly affects the carbonation degree of calcium-bearing hydrates.

This study proposes a wet–dry cycle carbonation method (dripping technique, which periodically drips water on waste concrete) to improve the carbonation efficiency of the smallest particles, around 1 mm, produced after crushing waste concrete in an intermediate treatment plant without additional crushing. The carbonation degree achieved through the dripping technique was compared and analysed with that achieved through the semi-dry carbonation process. The amount of CO_2 absorbed and the polymorphs of calcium carbonate were evaluated through thermogravimetric analysis (TGA), powder X-ray diffraction (XRD), and Fourier transform infrared spectroscopy in attenuated total reflection mode (FTIR-ATR). The textures of the cross-sections of the particles after carbonation were characterised through scanning electron microscopy (SEM) and electron dispersive spectroscopy (EDS).

2. Materials and Methods

2.1 Materials

This study used laboratory-made cement paste to mimic the binder part of waste concrete and dissolve the disproportion based on the difference in the amount of aggregate in the waste concrete. Cement provided by the Japan Cement Association was used as cement paste with a water-to-cement ratio of 0.6. The hardening cement paste was remixed every 1 h for 8 h to minimize bleeding and segregation. The cement paste underwent sealed curing for over 6 months at 20 °C. After curing, the hardened cement paste was crushed using a ball mill and sieved under a nitrogen atmosphere. To mimic the size of finely crushed hardened cement paste detached from concrete waste at an actual demolition site in Japan, the target particle size of the hardened cement fine (HCF) was set between 0.6 mm and 1.18 mm. Tables 1 and 2 show the chemical compositions of the cement provided by the Japan Cement Association and the mineral compositions of the cement from the XRD measurements, respectively.

Table 1. Chemical compositions (wt%) of cement.

	SiO_2	Al_2O_3	Fe_2O_3	CaO	MgO	SO_3	Na_2O	K_2O	TiO_2	ig. loss
Cement	21.41	4.84	3.20	65.01	1.08	2.02	0.33	0.43	0.24	0.97

Table 2. Mineral compositions (wt%) of cement.

	C_3S	C_2S	C_3A	C_4AF	Gypsum	Basanite	Periclase	Calcite	Amorphous
Cement	65.2±1.2	12.6±2.3	5.8±0.3	6.3±0.3	1.7±0.4	1.54±0.14	0.37±0.19	0.25±0.13	6±2

2.2. Methods

2.2.1. Experiment conditions

The HCF was placed on the filter, and water was dripped on it for 30 s at regular intervals. In the first cycle, distilled water was supplied as a dripping solution. However, from the second cycle, a bicarbonate solution, dissolved CO_2, was suppplied owing to the circulation of the dripping solution. To analyze the effect of the wet-dry cycle on the degree of carbonation of particles, samples were prepared where water was dripped at 24-hour intervals, which was sufficient to dry the particles, and at 12-hour intervals, which was halved. In addition, to compare the amount of CO_2 absorbed through the dripping technique with the semi-dry carbonation process, HCF samples were prepared at a constant RH of 60 % (intermediate RH) or 85 % (high RH). Figure 1 shows a schematic of the dripper device. The mass of each sample and volume of the dripping solution for 30 s were 1.5 g and 4 ml, respectively. The room temperature and CO_2 concentration were 20 ℃ and 0.04–0.05 %, respectively. Table 3 shows the experimental conditions.

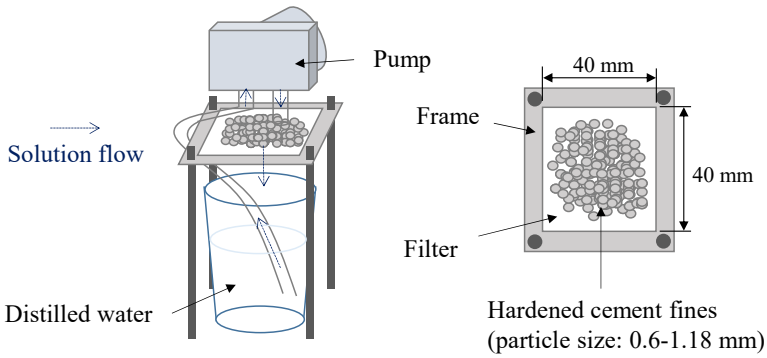

Figure 1. Schematic illustration of dripper device for CO_2 adsorption

Table 3. Experiment conditions

Particle size of HCF		0.6–1.18 mm
Water-to-cement ratio		0.6
Dripping	Duration/Interval	30 s / 24 h, 12 h (Room condition: 20 ℃, 60 % RH)
Semi-dry	Conditions	60 % RH, 85 % RH (temperature: 20 ℃)
CO_2 concentration		0.04–0.05 % (concentration in the atmosphere)
Carbonation periods		0, 1, 3, 7, 14, 28 days

1

2 *2.2.2. Thermogravimetric analysis* (*TGA*)

3 The amount of CO_2 absorbed by the HCF was determined through TGA. Carbonation was carried
4 out for 0, 1, 3, 7, 14, and 28 d under each condition, followed by the TGA. Before conducting the TGA,
5 the carbonated HCF was dried for over 24 h in a vacuum desiccator. The measurement was performed
6 under an N_2 atmosphere at 20 ℃ to 950 ℃ with a heating rate of 10 ℃/min. The sample amount was
7 15 ± 0.05 mg and the samples were maintained at 105 ℃ for 30 min for drying and at 950 ℃ for 1 h
8 for dehydrating the silica gel and C-S-H.

9 In this study, a differential thermogravimetry (DTG) graph was used to interpret the TGA results and
10 calculate the weight loss from the $Ca(OH)_2$ decomposition and the CO_2 emissions from the calcium
11 carbonate decarbonisation. The temperature–DTG graph reflects the weight loss of the sample over a
12 given temperature range. C-S-H decomposes over a wide temperature range, from 30 ℃ to 900 ℃
13 [16,17]. Therefore, to exclude the weight loss from C-S-H decomposition in the temperature range of
14 calcium carbonate decarbonisation and $Ca(OH)_2$ decomposition, the CO_2 emissions and $Ca(OH)_2$
15 amounts of the samples were calculated using the tangential method [18].

16 The amount of $Ca(OH)_2$ and $CaCO_3$ in each sample was normalized to 100 g of cement using Eqs.
17 (2) and (3) [6]

18

19 $$m_{CH,\,norm} = \frac{m_{CH}}{m_{950}} \times m_{950,cem} \quad (2)$$

20 $$m_{CC,\,norm} = \frac{m_{CC}}{m_{950}} \times m_{950,cem} \quad (3)$$

21

where, $m_{CH,norm}$ and $m_{CC,norm}$ are $Ca(OH)_2$ and $CaCO_3$ amounts per 100 g of cement, respectively, m_{CH} and m_{CC} are $Ca(OH)_2$ and $CaCO_3$ amount per 100 g of HCF, respectively, $m_{950,cem}$ is ignited mass of cement at 950 ℃, m_{950} is ignited mass of each sample at 950 ℃.

Base on the normalized value, degree of carbonation of $Ca(OH)_2$ and HCF were calculated using Eqs. (4) and (5)

$$DoC_{CH}(\%) = \frac{m_{CH0,norm} - m_{CH,norm}}{m_{CH0,norm}} \times 100 \quad (4)$$

$$DoC_{HCF}(\%) = \frac{m_{CC,norm} \times \frac{56}{100}}{m_{CaO,cem}} \times 100 \quad (5)$$

where, DoC_{CH} is degree of carbonation of $Ca(OH)_2$, DoC_{HCF} is degree of carbonation of HCF, $m_{CaO,cem}$ is weight fraction of CaO in cement, $m_{CH0,norm}$ is $Ca(OH)_2$ amount per 100 g of cement before carbonation.

2.2.3. X-ray diffraction (XRD) and Rietveld analysis

Powder XRD and Rietveld analyses were conducted to confirm the phase changes caused by each carbonation process after 0, 3, 7, 14, and 28 d of carbonation. The measurements were performed on a SmartLab (Rigaku, Japan) with Cu-Kα radiation at 45 kV tube voltage and 200 mA tube current. The measurement conditions were as follows: 2θ = 5–70 ° scanning range, 0.02 ° step width and 2 °/min scanning speed. For the non-carbonated samples, hydration was terminated using the solvent exchange method using isopropanol (IPA). The non-carbonated samples were submerged in IPA for 1 d and then filtered from the IPA solution using a filtration funnel with filter paper and an aspirator. The samples were stored in a desiccator at 20 ℃ and 11 % RH, maintained by circulating air passed through LiCl saturated solution and CO_2 absorbent for 14 d to remove any remaining IPA. The carbonated samples were oven-dried at 105 ℃ for 48 h. It should be noted that oven-drying leads to a partial C-S-H dehydration and decomposition of AFm and AFt [19-21]. According to D. Snoeck et al., since carbonated hcp also showed similar trends to oven-dried hcp [20], this study adopted the oven-drying

method for carbonated HCF. The dried samples were ground to <150 μm using an agate mortar. Rietveld analysis was performed to quantitatively determine the phase composition of each carbonated sample. The powdered sample was mixed with 10 wt% α-Al_2O_3 as an internal reference, and the results were analysed using SmartLab Studio II by Rigaku. The phases considered for the non-carbonated sample were alite, belite, ferrite, calcite, portlandite, ettringite, monosulfoaluminate, hemicarboaluminate, hydrogarnet and corundum. For carbonated samples, alite, belite, ferrite, calcite, vaterite, portlandite, hemicarboaluminate, monocarboaluminate (not detected), hydrogarnet and corundum were considered. The results were expressed in weight fraction.

2.2.4. Fourier transform infrared spectroscopy (*FTIR*)

Fourier transform infrared spectroscopy in attenuated total reflection mode (FTIR-ATR) was performed after carbonation for 0, 1, 3, 7, 14, and 28 d under each condition. Similar to the TGA, the carbonated HCF was dried for over 24 h in a vacuum desiccator before the analysis. FTIR spectra were recorded on an FT/IR 4700 (JASCO) instrument ranging from 650 cm^{-1} to 4000 cm^{-1} with a resolution of 4 cm^{-1}. The data were recorded as % transmission, and an average of 128 scans was taken.

2.2.5. Scanning electronic microscopy and electron dispersive spectroscopy (SEM-EDS)

The morphologies of the HCF carbonated under different conditions were characterised through scanning electron microscopy and electron dispersive spectroscopy (SEM-EDS, Hitachi, TM4000Plus). The SEM samples were dried for over 7 d in a vacuum desiccator and then impregnated with an epoxy resin under vacuum. The samples were polished using silicon carbide (P1200), diamond suspensions (6 μm and 1 μm), and fumed silica (0.2 μm) under an alcohol-based lubricant. Overall polishing steps used only alcohol-based lubricant, and isopropanol (or ethanol) was used for sonication process between polishing steps. After polishing, the samples were dried for approximately 24 h in a vacuum desiccator. The observations were made at an accelerating voltage of 15 kV and a working distance of 8.5–8.6 mm. To prevent charging, a 10–15 nm-thick carbon layer was coated onto the surfaces of the samples before observation.

The EDS hypermaps were acquired at a resolution of 1024 × 768 pixels. The dwell time was 256 s/pixel, averaging three frames. Under these conditions, the map acquisition time was approximately 10 min. To perform quantitative EDS analyses, certified standards were used for Si, Mg, Fe, Al, Ca, S, K, and Na.

2.2.6. Image analysis for porosity estimation

Image analysis was conducted to clarify the migration of calcium ions by confirming the location of relatively large voids, which expressed as porosity in Figure 9, created owing to the migration of calcium ions and drying through the dripping process. The SEM images, having a resolution of 2560 × 1920 pixels, were analyzed for porosity estimation using ImageJ software. The sizes of a pixel by the scale factors, which to check the aspect of the whole particle, were 0.47μm (x100) for Drip_12h, Drip_24h, and RH60, and 0.26μm (x180) for RH85. The "Auto Threshold" function was used, and the "Minimum" Auto Threshold type was selected to determine the porosity.

3. Results

3.1 Thermogravimetric analysis (*TGA*)

Figures 2 and 3 show the TGA results and carbonation degree of the HCF by period obtained from the TGA results, respectively.

Carbonation was accelerated in the solution-dripped sample in the early stages. After 1 d of carbonation, the carbonation degree of the HCF with the 12-hour dripping interval was over twice that at 60 % RH and 1.4 times higher than at 85 % RH. In the case of Drip_24h, the carbonation degree of the HCF after 1 d of carbonation was nearly the same as that at 85% RH. However, after 3 and 7 d of carbonation, the carbonation degree of the HCF was 1.7 and 2 times higher than that at 85 % RH, respectively. Notably, changes in the internal microstructure occurred during the first wet–dry cycle, and the altered microstructure promoted carbonation from the second cycle. This is further discussed in Section 4.2.

The results show that after 14 d of carbonation, nearly all the $Ca(OH)_2$ in the sample, where the

solution was dripped once in 24 h, was consumed. However, in the case of Drip_12h, $Ca(OH)_2$ carbonation was observed to be extremely slow after 3 d of carbonation. At 60 % RH, C-S-H and $Ca(OH)_2$ were more decomposed than at 85 % RH after 14 d of carbonation. As shown in Figure 2, the calcium carbonate generated at 60 % RH was decomposed at a lower temperature range, indicating that calcium carbonate with low crystallinity was generated. Thus, metastable calcium carbonate was primarily generated in the sample carbonated at 60 % RH. This result is consistent with the results of other researchers who observed that poorly crystalline carbonates were primarily formed at 58 % RH in the early stage of carbonation [6].

As previously mentioned, the carbonation degree of Drip_12h was the highest after 3 d of carbonation and gradually decreased thereafter (Figure 3). Similarly, in the case of Drip_24h, the carbonation degree was the highest after 14 d of carbonation and decreased after 28 d of carbonation. However, calcium carbonate does not undergo decarboxylation at room temperature and high pH. This indicates that during the carbonation process using the dripping technique, where the solution was dripped periodically, the calcium carbonate generated on the surface came off by the solution (Figure 4) or might pass through the filter with the solution. Therefore, the carbonation degree of the HCF is presumed to decrease when the amount of calcium carbonate falling into the solution is greater than the amount of newly generated calcium carbonate (between 3–7 ds for Drip_12h and 14–28 d for Drip_24h). To correct the carbonation degree, the minimum amount of calcium carbonate that fell was calculated based on the following two assumptions:

1. All the $Ca(OH)_2$ that had decreased since the period of maximum carbonation degree were carbonated, generating calcium carbonate.
2. C-S-H was uncarbonated after the maximum carbonation degree period. (It should be noted that this assumption does not actually mean that C-S-H was uncarbonated after the maximum carbonation degree period.)

Figure 3(b) shows the results. The minimum carbonation degree is represented with the assumption that C-S-H was uncarbonated after 3 d (for Drip_12h) and 14 d (for Drip_24h). Nevertheless, the carbonation degree of the HCF increased because it reflected the calculated calcium carbonate

1 production amount from the calcium hydroxide reduction amount.

2

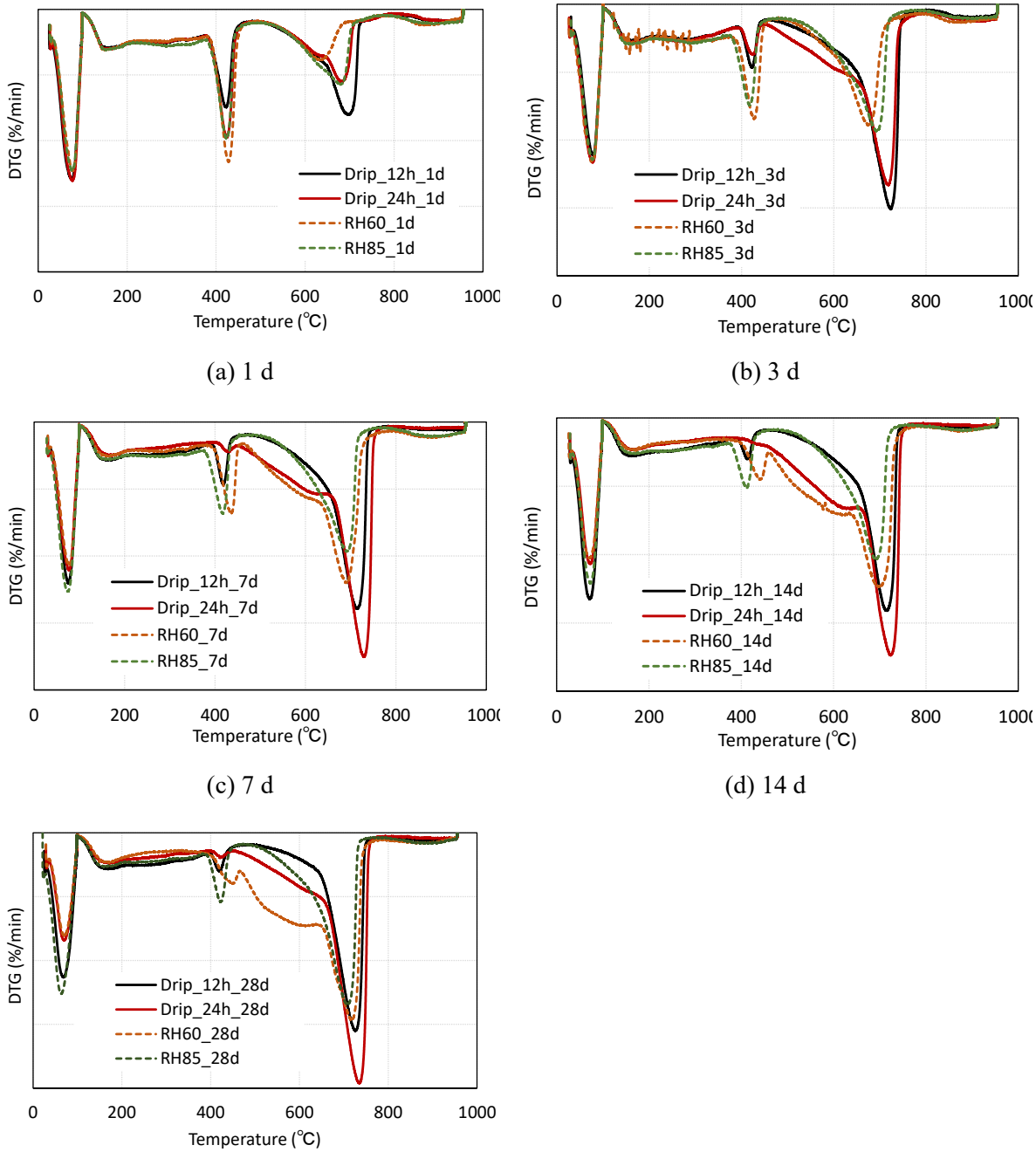

(a) 1 d (b) 3 d

(c) 7 d (d) 14 d

(e) 28 d

Figure 2. TGA results

3

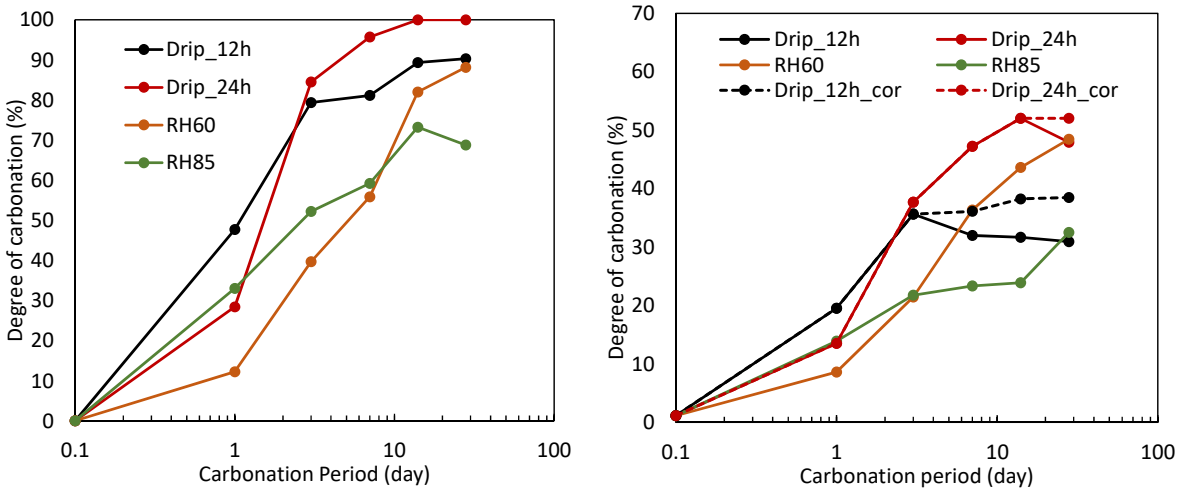

(a) $Ca(OH)_2$ (b) Average

Figure 3. Carbonation degree by period

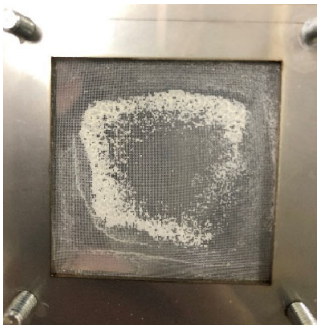

Figure 4. Remained calcium carbonate on the filter after 28 d of carbonation

3.2 X-ray diffraction (XRD) and Rietveld analysis

Figure 5 shows the XRD results. This section interprets the graph by focusing on the change in the $Ca(OH)_2$, calcite, and vaterite peak intensity as the carbonation progresses. First, in the case of Drip_12h, the difference in the $Ca(OH)_2$ and calcite peaks as carbonation progressed was insignificant, and the vaterite peak was barely noticeable. For Drip_24h, the $Ca(OH)_2$ peak that existed until 3 d of carbonation nearly disappeared after 7 d. The calcite peak increased with time. The vaterite peak appeared after 7 and 14 d of carbonation but was barely observed after 28 d of carbonation. This is because vaterite, a metastable phase, changes into calcite, a stable phase, through repeated dissolution and reprecipitation reactions [22-23]. Therefore, vaterite, which in the solution dripped samples or samples at high RH, was changed into calcite. Meanwhile, according to Drouet et al. [10], the lack of pore water at a low RH suppresses the polymorphic transformation from a metastable state to a

thermodynamically stable state. At 60 % RH, the $Ca(OH)_2$ peak decreased over time, and the calcite and vaterite peaks increased. These results suggest that the peak at approximately 450–650 ℃ in the TGA mentioned in Section 3.1 is attributed to the vaterite decomposition. Lastly, at 85 % RH, the rate of $Ca(OH)_2$ consumed over time was smaller than that in other conditions. The vaterite peak was hardly observed, and the calcite peak intensity increased.

Rietveld analysis was performed based on the XRD results. Figure 6 shows the results. Under all carbonation conditions, the proportion of $Ca(OH)_2$ tended to decrease over time. In particular, for Drip_24h, most of the $Ca(OH)_2$ was carbonated after 7 d. The proportion of the amorphous containing C-S-H decreased as carbonation progressed at Drip_24h and 60 % RH. By contrast, at 85 % RH, it exhibited minimal changes. In the case of Drip_12h, the ratio of the amorphous phase in the early stage decreased over time but increased again after 14 d of carbonation. Calcite and vaterite formed in the calcium carbonate phase under all carbonation conditions. Calcite was produced most abundantly in Drip_24h, whereas vaterite was most abundant at 60 % RH.

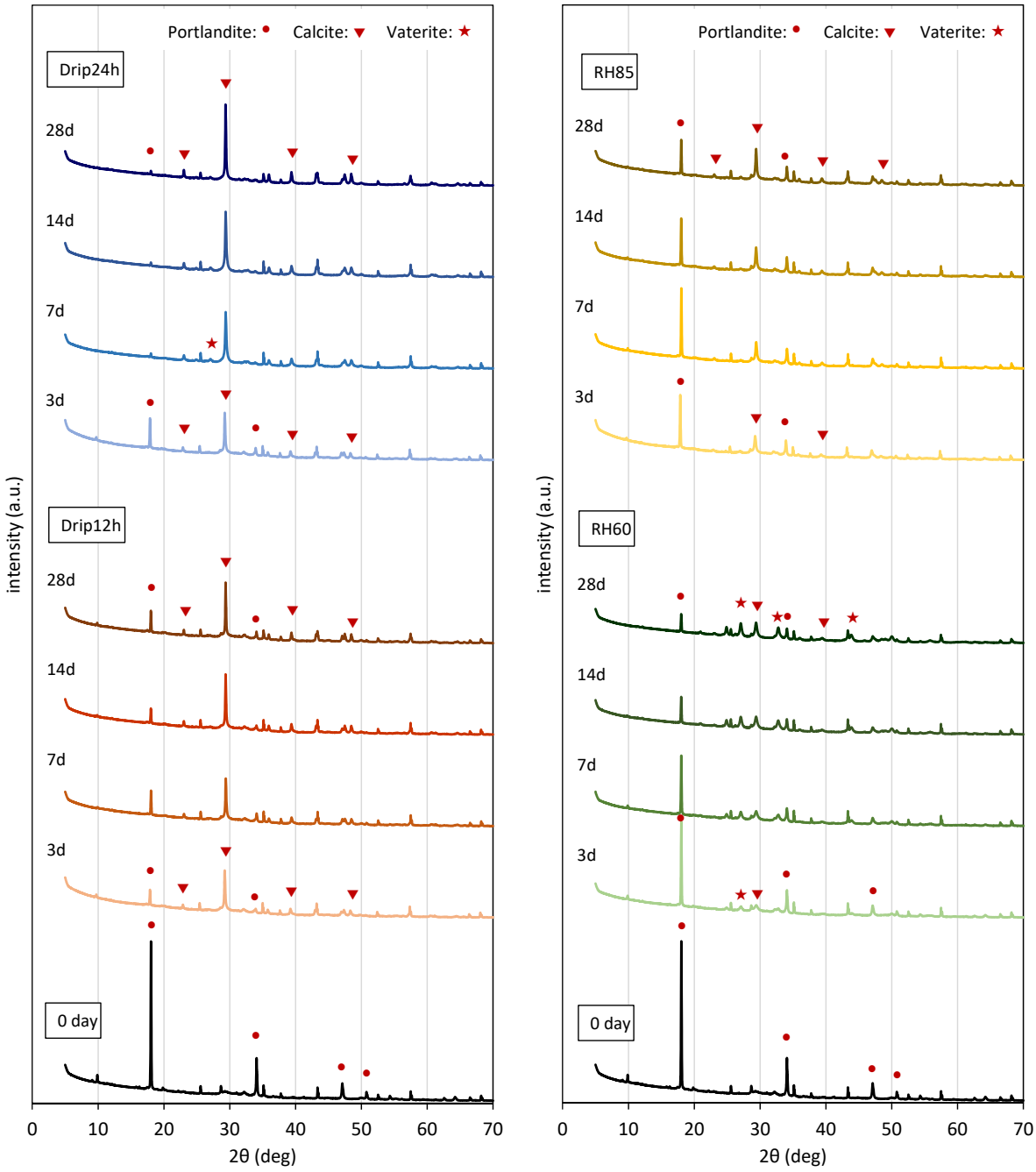

(a) Dripping technique (b) Semi-dry

Figure 5. XRD measurement results

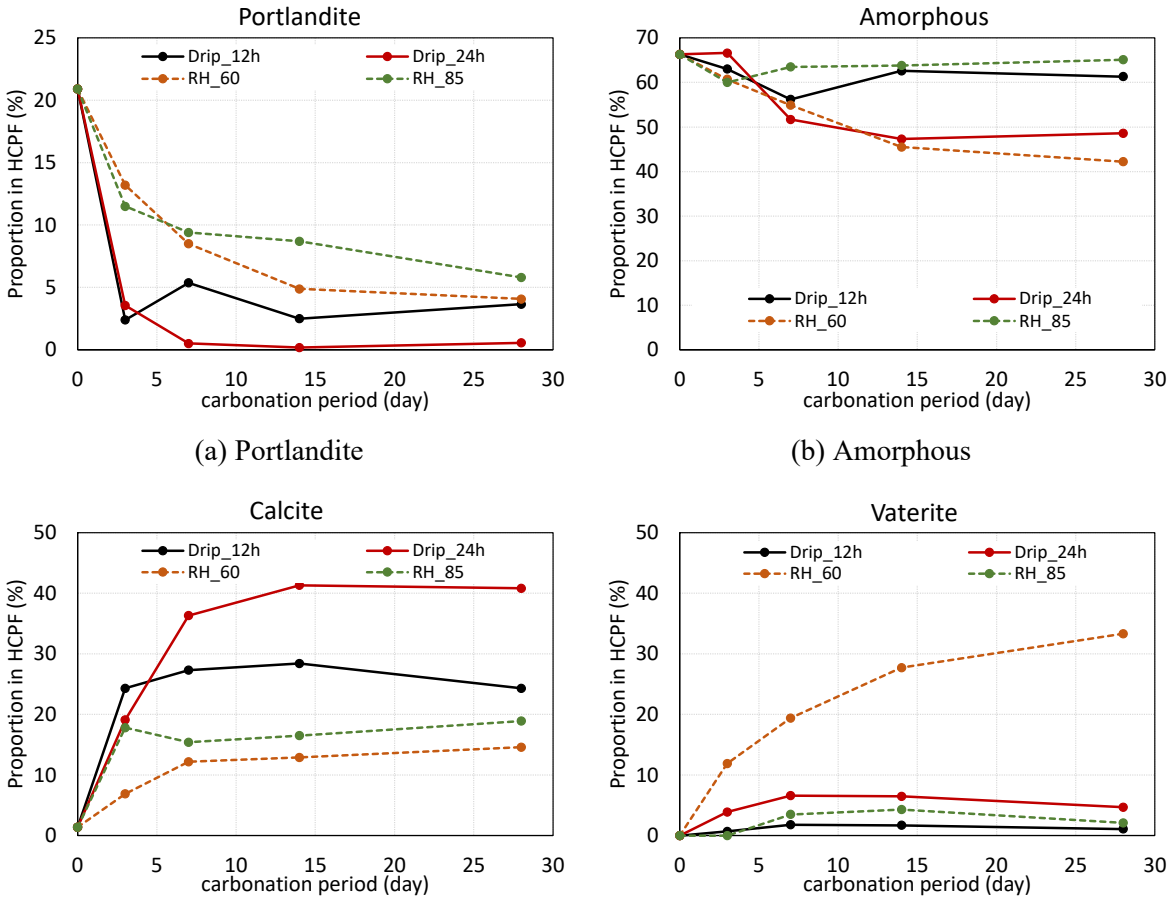

(a) Portlandite (b) Amorphous

(c) Calcite (d) Vaterite

Figure 6. Rietveld analysis results

3.3. Fourier transform infrared spectroscopy (FTIR)

The FTIR spectra of carbonates show several typical absorption bands, including asymmetric C–O-stretching (ν3), CO_3^{2-}-bending (ν2), and O–C–O-bending (ν4) at approximately 1420 cm^{-1}, 870 cm^{-1}, and within a range of 700–746 cm^{-1}, respectively [7,24,25]. The silica compounds show the main absorption band between 800–1200 cm^{-1} [26-29]. The Si-O stretching band appears around 950 cm^{-1}; when the Ca/Si ratio of C-S-H decreases, the peak shifts to higher wavenumbers [28,29].

In this study, to observe the flow of bonding changes in each series over the carbonation time, normalisation was performed by setting the area in the range of 1600–1700 cm^{-1} to 1 after baseline correction. Figure 7 shows the results. In all samples, calcite peaks were observed at approximately 1420, 870, and 720 cm^{-1}. For Drip_12h, the C-S-H peak did not change significantly at approximately 960 cm^{-1}. However, the silica gel peak between 1050 cm^{-1} and 1150 cm^{-1} occurred after 1 d of

carbonation. C-S-H rapidly decomposed owing to the wet–dry cycles, producing silica gel. For Drip_24h, after 14 d of carbonation, the vaterite peak occurred at approximately 740 cm^{-1}, and the C-S-H peak also shifted to higher wavenumbers. At 60 % RH, unlike other series, the C-S-H peak shift phenomenon was evident over time. In addition, a silica gel peak was observed in the sample after 7 d of carbonation. Vaterite peaks were also observed at approximately 1490 and 740 cm^{-1}. These results suggest that as carbonation progresses at 60 % RH, vaterite and calcite were generated owing to $Ca(OH)_2$ decomposition and C-S-H decalcification, and silica gel was generated owing to C-S-H decomposition. At 85 % RH, the Ca/Si ratio of C-S-H hardly changed. Moreover, the $Ca(OH)_2$ decomposition increased the calcite production. Similar to the TGA and XRD results, a decreasing trend in the amount of vaterite was observed in the solution-dripped and 85 % RH samples.

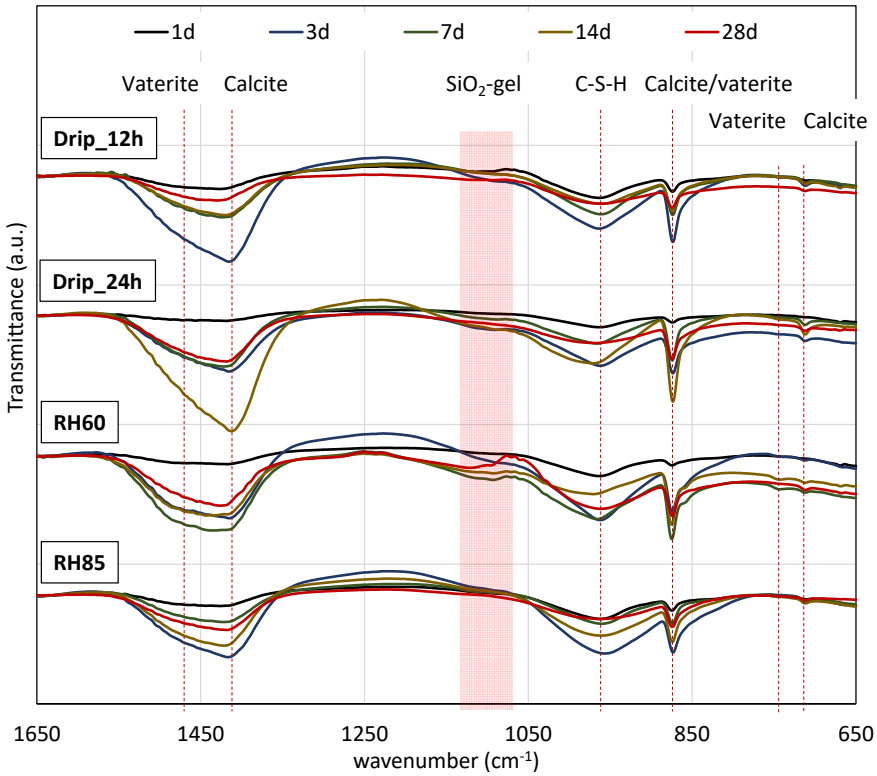

Figure 7. FTIR measurement results

3.4 Scanning electronic microscopy and electron dispersive spectroscopy (SEM-EDS)

Figure 8 shows the cross-sectional texture images after 7 d of carbonation. From the SEM images, layers on the surface were observed in the Drip_12h and Drip_24h samples. The EDS analysis showed

that calcium was distributed on the particle surface in Drip_12h and Drip_24h. As shown in Figure 2, after 7 d of carbonation, a minimal amount of $Ca(OH)_2$ remained in the solution-dripped samples, indicating that most of the calcium on the surface precipitated as calcium carbonate. The ions precipitate at the liquid/vapour interface, leading to solid growth [30]. In this scenario, as the surface dried, calcium ions released from the calcium-bearing hydrates dissolved by the dripping solution reacted with carbonate ions, precipitating calcium carbonate on the particle surface, which is the liquid/vapour interface. A comparison of Drip_12h and Drip_24h revealed that the calcium carbonate layer was thicker on the particle surface of Drip_12h. However, in the cross-sections of the samples carbonated in the semi-dry carbonation process, the layer could not be observed on the surface.

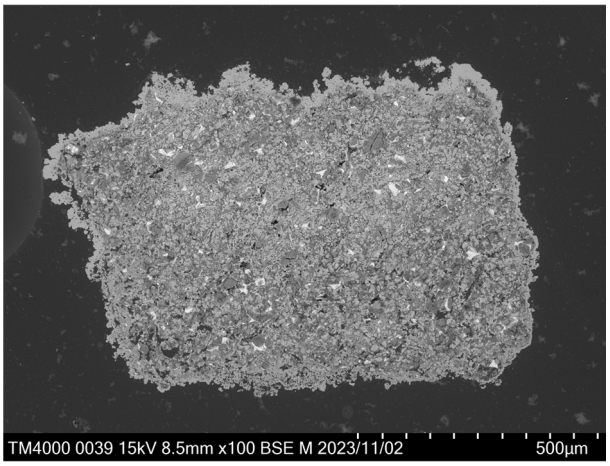

(a) Drip_12h_7d (SEM image, x100)

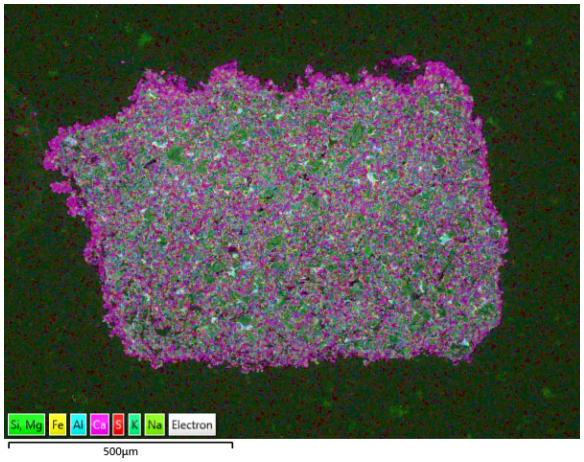

(b) Drip_12h_7d (EDS mapping, x100)

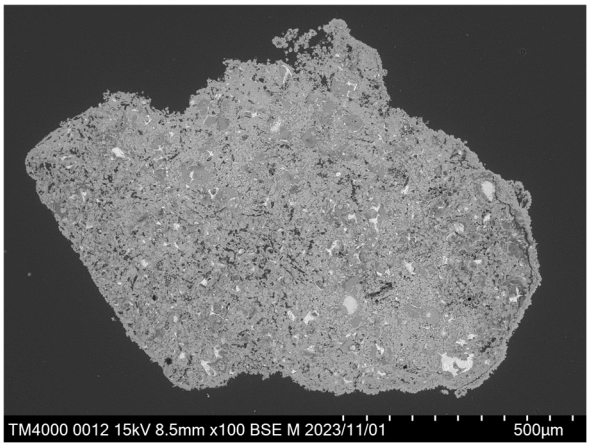

(c) Drip_24h_7d (SEM image, x100)

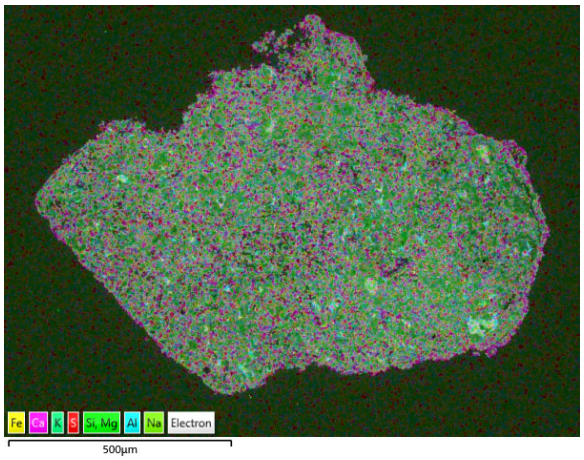

(d) Drip_24h_7d (EDS mapping, x100)

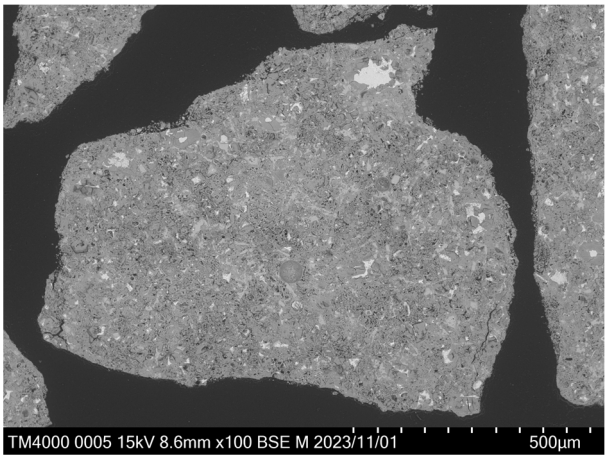

(e) RH60_7d (SEM image, x100)

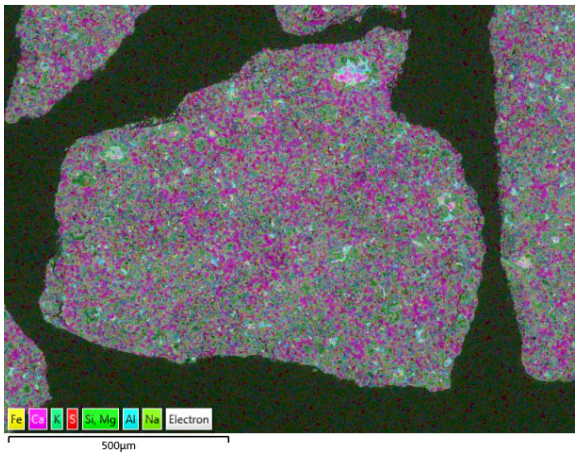

(f) RH60_7d (EDS mapping, x100)

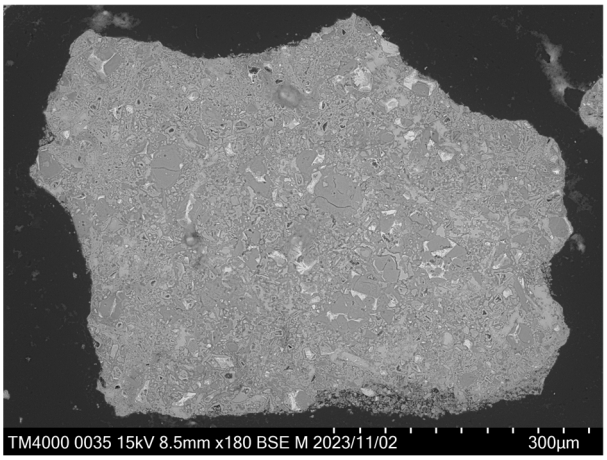

(g) RH85_7d (SEM image, x180)

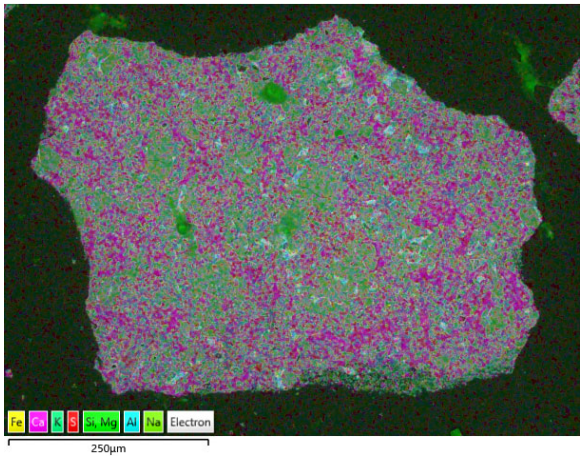

(h) RH85_7d (EDS mapping, x180)

Figure 8. SEM-EDS mapping images of carbonated HCF

As shown in Figure 8, for the solution-dripped samples, large pores were observed inside the particles, whereas pores were barely detected at 85 % RH. To investigate the effects of the wet–dry cycle and humidity environment on the internal structure of the particles, the SEM images shown in Figure 8 were analysed to estimate the porosity. The grayscale values of Drip_12h, Drip_24h, RH60, and RH85 adopted in this study were 84, 81, 76, and 80, respectively, obtained when “Minimum” was selected as the Auto Threshold type. The ImageJ software features 17 Auto Threshold types, and each grayscale value is shown in Appendix A.

Figure 9 shows the results of the imaging analysis. Drip_12h had the highest porosity of 6.181 %, whereas RH85 had the lowest porosity of 0.611 %. Large voids were observed in the solution-dripped samples, and Drip_12h was larger and had more pores than Drip_24h. Moreover, compared with the

results of RH60 and RH85, twice as many pores were observed at 60 % RH than at 85 % RH.

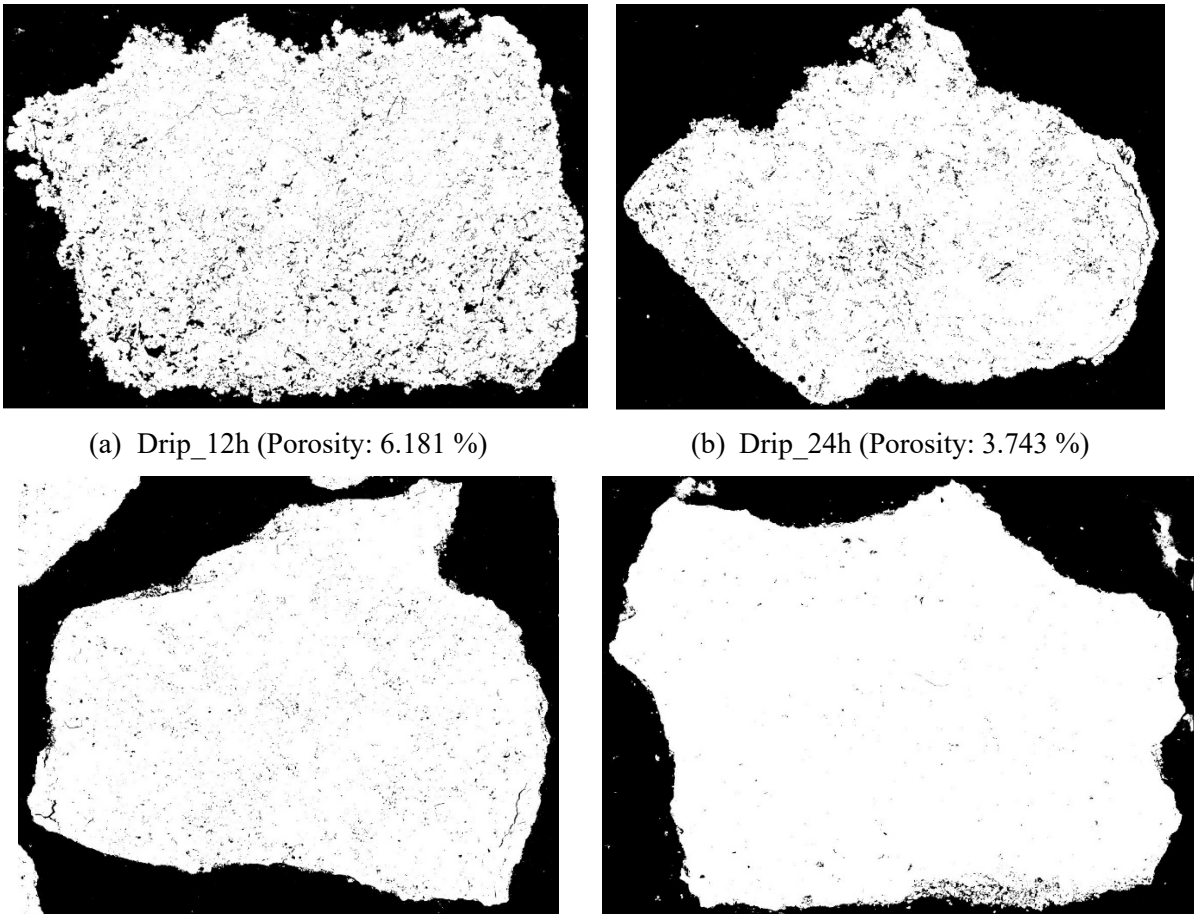

(a) Drip_12h (Porosity: 6.181 %) (b) Drip_24h (Porosity: 3.743 %)

(c) RH 60 (Porosity: 1.321 %) (d) RH 85 (Porosity: 0.611 %)

Figure 9. Imaging analysis results

4. Discussions

4.1 Relationship between carbonation conditions and carbonation of calcium-bearing hydrates

To investigate the relationship between the carbonation conditions in this study and the carbonation of calcium-bearing hydrates, the calcium carbonate fraction caused by the carbonation of each calcium-bearing hydrate was calculated from the TGA results. Figure 10 shows the results.

In semi-dry carbonation process, carbonation of $Ca(OH)_2$ progressed rapidly at 85 % RH in the early stage, resulting in a greater degree of carbonation than at 60 % RH. As time passed, it was found that the carbonation of C-S-H as well as $Ca(OH)_2$ progressed at 60 % RH, but the carbonation degree of $Ca(OH)_2$ and C-S-H was barely changed at 85 % RH. When $Ca(OH)_2$ is carbonated, porosity decrease

because volume of calcium carbonate precipitated by carbonation of $Ca(OH)_2$ is larger than the volume of $Ca(OH)_2$ [31,32]. In addition, calcium carbonate precipitated around $Ca(OH)_2$ crystals can inhibit or slow down further dissolution [33,34]. The pore filling effect and protective layer could be the reason for carbonation stagnates at 85 % RH. When C-S-H is carbonated, calcium would be decalcified to precipitate as calcium carbonate with the formation of amorphous calcium modified silica gel [35-37]. This reaction is accompanied by an overall decrease in solid volume and an increase in porosity and pore sizes [31,34]. The increase in porosity and pore size due to carbonation, which makes the diffusion of CO_2 easier, is one of the reasons for carbonation to proceed steadily at 60 % RH.

As previously mentioned, the dripping technique was limited in that it was difficult to determine the amount of calcium carbonate from C-S-H carbonation owing to calcium carbonate falling into the solution. Nevertheless, in Drip_24h, the amount of calcium carbonate from the $Ca(OH)_2$ carbonation was higher than that at 60 % RH and 85 % RH. Moreover, calcium carbonate production due to the C-S-H carbonation was also enhanced, improving the overall carbonation degree.

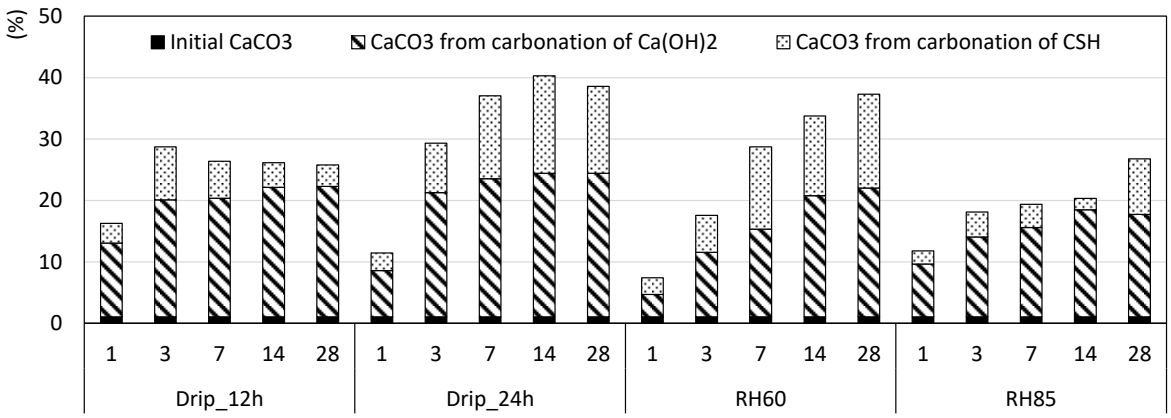

Figure 10. Calcium carbonate in the HCF from the carbonation of calcium-bearing hydrates

4.2 Carbonation rate of HCF with different environments

Figure 11 shows the thermodynamic equilibrium calculation results for the carbonation of the hardened cement paste used in this experiment using the Gibbs free energy minimization software GEMS. The mineral composition of cement as input data was obtained from Rietveld analysis as shown in Table 2. To simulate carbonation, the amount of CO_2 reacting was increased from 0 to 50 g per 100

g cement. The graph also shows the relationship between pH and Ca and Si ion concentrations in the pore solution during carbonation.

Before interpreting the graph, it is essential to understand the forms in the solution based on the pH when CO_2 is dissolved, described as follows [38]: 1) At a pH higher than 12, it exists as carbonate ions; 2) As the pH decreases, the fraction of bicarbonate ions increases, reaching its peak at pH 8; 3) When the pH drops below 8, the lower the pH, the higher the fraction in the form of carbonic acid. When the pH reaches approximately 4, it exists solely in the form of carbonic acid.

Because non-carbonated HCF has a pH of over 13 owing to $Ca(OH)_2$ and other alkaline materials [39], CO_2 gas dissolved in the pore solution exists as carbonate ions; these carbonate ions first cause $Ca(OH)_2$ decomposition and C-S-H decalcification. C-S-H decalcification proceeded until the Ca/Si molar ratio reached 0.67 [35]. Furthermore, a constant pH was maintained, and the calcium and silica ion concentrations were nearly constant. When all the $Ca(OH)_2$ was consumed, the pH gradually decreased. Subsequently, C-S-H decomposed to form calcium carbonate and calcium-modified amorphous silica gel, increasing the concentration of silica ions. Finally, all the C-S-H was decomposed, and the concentrations of calcium and silica ions temporarily decreased. However, as the pH decreased below 7, the bicarbonate ions decreased, carbonic acid increased, and calcium carbonate dissolved in the carbonic acid, increasing the concentration of calcium ions.

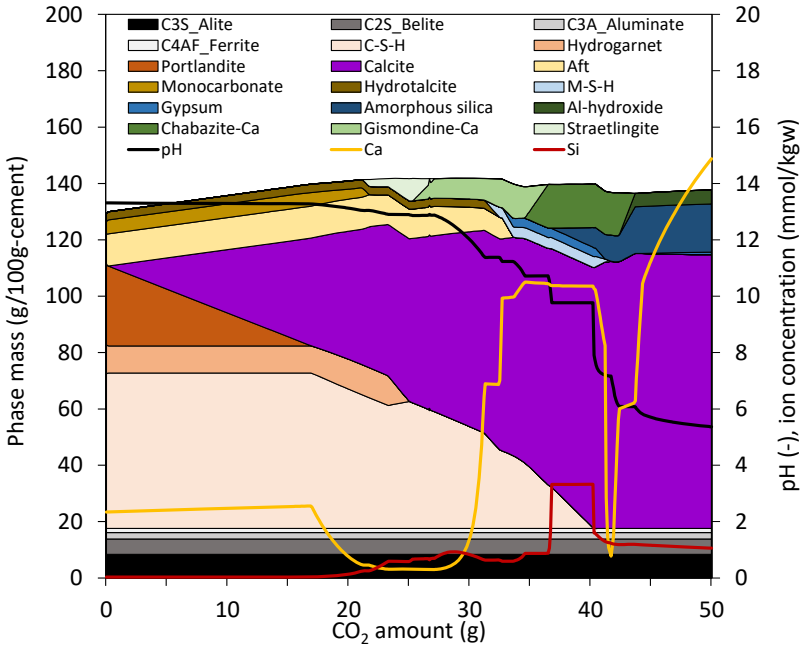

Figure 11. Thermodynamic modelling of the carbonation process

Based on these results, the differences in the carbonation mechanisms using semi-dry and dripping techniques are discussed. To understand this, the focus should be on the amount of solution per unit of time infiltrating the particle, CO_2 diffusion, and migration of calcium ions released by the $Ca(OH)_2$ decomposition and C-S-H decalcification. The ease of infiltration of the solution into the non-carbonated HCF particles depends on the drying history. During drying, the C-S-H sheets in the sample move and shrink owing to the capillary tension of the pore solution or surface energy acting on the C-S-H sheet [40,41]. This rearrangement of C-S-H sheets generates a number of capillary pores and enhances their continuity [6,41,42]. For carbonated HCP particles, the ease of infiltration depends on the type of carbonated calcium-bearing hydrates and the drying history, as discussed in Section 4.1.

In semi-dry carbonation, calcium-bearing hydrates, such as $Ca(OH)_2$ and C-S-H, are dissolved in the pore solution, releasing calcium ions, and CO_2 diffuses into the particles and dissolves in the pore solution to form carbonate ions. These carbonate and calcium ions dissolved in the pore solution react and precipitate calcium carbonate on the surface of the calcium-bearing hydrates [43-45]. As previously mentioned, water dissolves calcium-bearing hydrates and releases calcium ions but hinders CO_2 diffusion; thus, the optimal RH for carbonation varies depending on the particle size. Regarding the particle size adopted in this study, the carbonation degree was higher at 85 % RH in the early stage of

carbonation and higher at 60 % RH after 14 d of carbonation.

By contrast, in the dripping technique, carbonation proceeded via the following mechanism: As shown in Figure 12, the carbonation period in the dripping technique could be divided into three sections.

During the first wet–dry cycle, when the solution was dripped onto the HCF particles, an aqueous film was formed around the particles, and the CO_2 in the air dissolved in the aqueous film, increasing the concentration of carbonate ions [Initial stage]. Furthermore, the dripping solution infiltrated the pores inside the particles, and calcium-bearing hydrates, such as C-S-H and $Ca(OH)_2$, were dissolved, releasing calcium ions. Subsequently, differences in calcium ion concentration occurred between the surface aqueous film and pore solution. This caused the calcium ions to migrate towards the surface. During the drying process, the HCF particles began to dry from the surface, and calcium ions reacted with carbonate ions on the surface and precipitated on the liquid/vapour interface. Moreover, during drying, pores were generated owing to the rearrangement of the C-S-H sheets.

As confirmed from the carbonation degrees of Drip_12h_1d and Drip_24h_3d, carbonation was accelerated from the second cycle [Accelerated stage]. This acceleration can be attributed to the following: 1) Rapid solution infiltration owing to the pores generated during the first cycle, particularly during the drying process, releasing larger amounts of calcium ions; 2) Owing to the difference in the calcium ion concentrations in the aqueous film on the surface and pore solution, calcium ions migrate more towards the surface. This promoted the growth of calcium carbonate crystals on the surface. As calcium carbonate was produced on the surface, silica gel remained inside, generating larger pores. As shown in Figure 11, the ion concentrations of the pore solution of the HCF calculated from thermodynamic equilibrium were 2.34 and 0.0377 (mmol/kgw) for Ca and Si, respectively. Therefore, numerous calcium ions migrated to the surface owing to the solution infiltrating the pores; however, owing to the low solubility of Si, their migration was limited, and they remained in the form of silica gel and then agglomerated through drying. As the wet–dry cycle progressed, the particles were divided by the calcium carbonate layer on the surface and agglomeration of silica gel inside, as shown in Figure 13.

Finally, the stagnation of carbonation was observed, as shown in Figure 3, between 3–7 d for

Drip_12h and 14–28 d for Drip_24h in the case of this study [Convergent stage]. This is because the density of the water-repellent calcium carbonate layer on the surface increased, and the thickness of the aqueous film decreased [46], resulting in prevented solution infiltration and CO_2 diffusion into the particle. In addition, while carbonation stagnated, the amount of calcium carbonate falling into the solution increased as the accumulated number of dripping cycles increased, reducing the carbonation degree.

Initial carbonation speed and the time to reach carbonation stagnation varied depending on the dripping interval. This is because the carbonation reaction in Drip_12h develops rapidly, forming a $CaCO_3$ layer ahead of Drip_24h and resulting in a slower subsequent carbonation reaction. Therefore, setting the dripping interval and drying conditions (surrounding RH) according to the particle size and total amount of carbonatable calcium inside the particles is necessary to efficiently apply and generalize the dripping technique. The specific surface area decreases as the particle size increases. Thus, the total amount of carbonatable calcium inside the particle increases, whereas the surface area on which calcium carbonate precipitates relatively decreases. Consequently, although many non-carbonated calcium-bearing hydrates remain inside, the HCF particles rapidly reach carbonation stagnation. Therefore, an increase in the particle size necessitates improving the carbonation degree by increasing the dripping interval or lowering the surrounding RH.

The proposed dripping technique offers promising advancements in accelerated carbonation rates in waste concrete recycling. Moreover, waste concrete carbonated through this technique can also be recycled as a raw material for calcium carbonate concrete, proposed by Maruyama et al. [47].

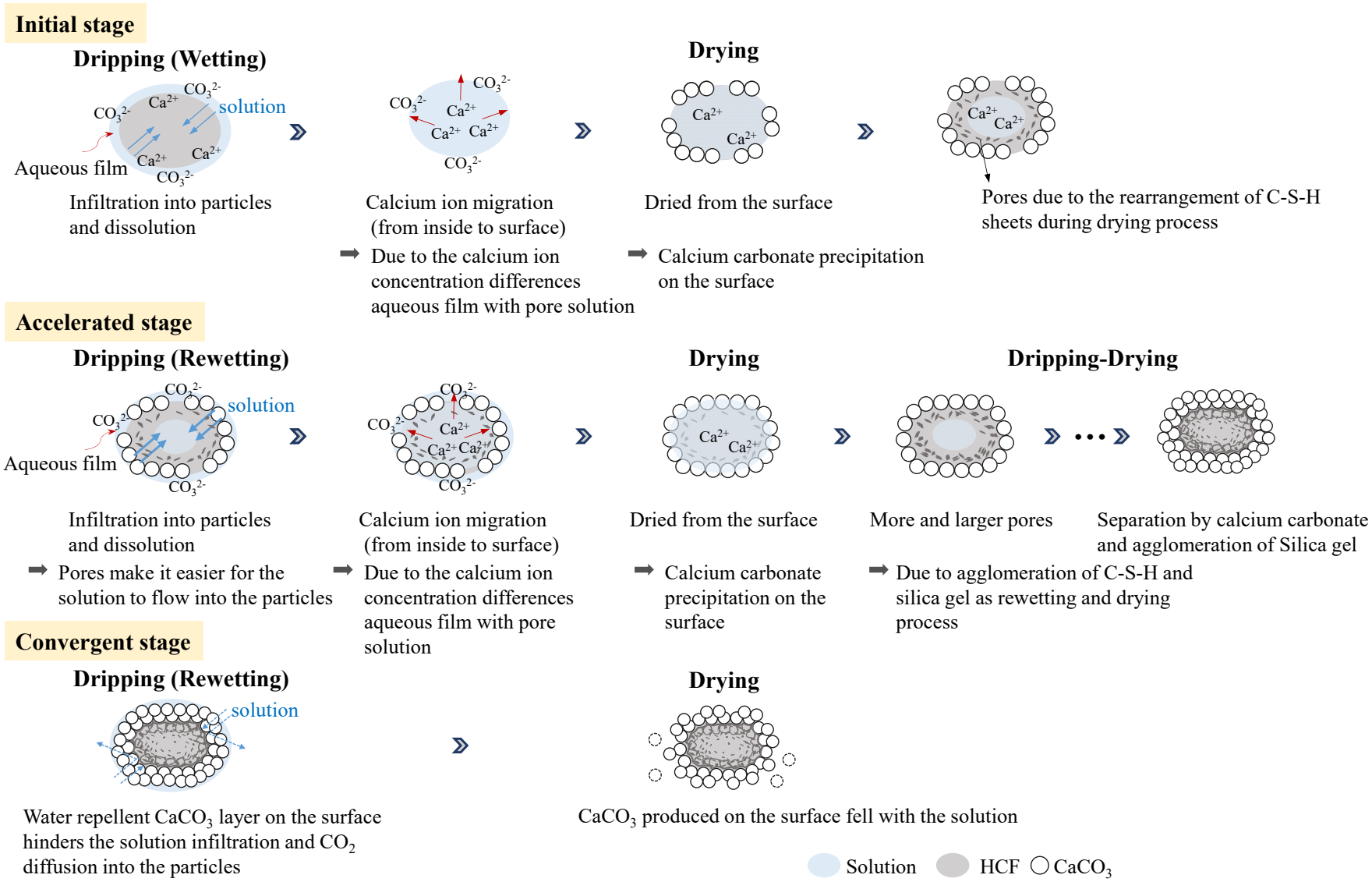

Figure 12. Schematic illustration of the carbonation-boosting mechanism by dripping technique

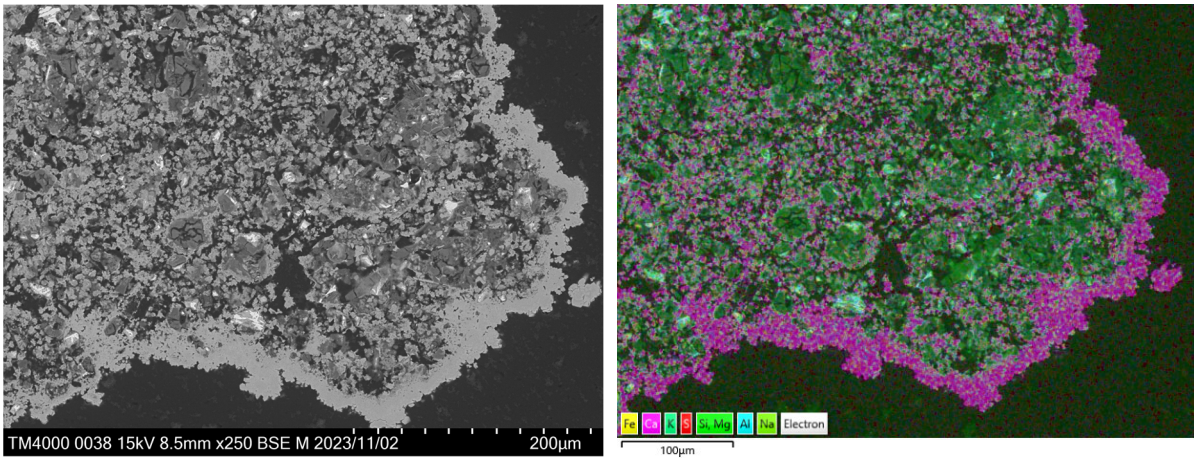

Figure 13. Calcium carbonate layer on the surface of Drip_12h_7d
(x250, left: SEM image, right: EDS result)

5. Conclusions

This study proposed a wet–dry cycle carbonation method (dripping technique) to improve the carbonation efficiency of HCF, mimicking the binder part of waste concrete, sized 0.6 mm to 1.18 mm. The carbonation degree achieved through the dripping technique was compared with that achieved with the semi-dry carbonation processes under atmospheric CO_2 concentration. The results of this study are summarised as follows:

1) From the SEM-EDS mapping images of the particles after 7 d of carbonation, calcium carbonate layers were observed on the surface of the solution-dripped particles. When the solution was dripped onto the HCF particles, an aqueous film was formed around the particles. The difference in the calcium ion concentration between the aqueous film and pore solution caused the calcium ions to migrate towards the surface. During drying, the HCF particles began to dry from the surface, and the migrated calcium ions reacted with the carbonate ions. This was because it precipitates on the liquid/vapour interface. By contrast, in semi-dry carbonation, the calcium ions did not migrate to the surface because an aqueous film was not formed on the particle surface. Thus, calcium carbonate precipitated inside the particles.

2) The results of the image analysis of the particles after 7 d of carbonation indicated that the porosity of solution-dripped samples was larger than that of the semi-dry carbonation samples, and large pores were detected inside the particles. This was because pores were generated owing to the rearrangement

of the C-S-H sheets during drying. In addition, owing to the difference in the solubilities of calcium and silica in the pore solution, the more calcium carbonate precipitated on the surface, the more silica gel remained inside, making the pores larger. A comparison between RH60 and RH85 revealed a higher porosity at 60 % RH owing to drying and C-S-H carbonation.

3) The TGA results after 1 d of carbonation revealed that the carbonation degree of the HCF with the 12-hour dripping interval was over twice that at 60 % RH and 1.4 times faster than at 85 % RH. For Drip_24h, the carbonation degrees of the HCF after 3 and 7 d of carbonation were 1.7 and 2 times faster than at 85 % RH, respectively.

4) For the solution-dripped samples, as the density of the water-repellent calcium carbonate layer on the surface increased, the thickness of the aqueous film decreased. Consequently, solution infiltration and CO_2 diffusion into the particle were prevented, stagnating carbonation. Therefore, setting the dripping interval and drying conditions (surrounding RH) according to the particle size and total amount of carbonatable calcium inside the particles is necessary to efficiently apply the dripping technique.

The proposed dripping technique offers promising advancements in accelerated carbonation rates in waste concrete recycling. In particular, creating wet-dry conditions using spring water at regular intervals to promote carbonation of waste concrete is a method that can be easily applied at intermediate waste treatment plants. Moreover, waste concrete carbonated through this technique can also be recycled as a raw material for calcium carbonate concrete, contributing to a sustainable construction society.

CRediT authorship contribution statement

Dayoung Oh: Data curation, Formal analysis, Methodology, Writing - original draft, Writing - review & editing. Ryoma Kitagaki: Conceptualization, Methodology, Supervision, Writing - review & editing. Takayoshi Masuo: Methodology. Zhijiang Li: Data curation. Ryo Kurihara: Data curation, Writing - review & editing. Takafumi Noguchi: Funding acquisition, Project administration, Writing - review & editing. Ippei Maruyama: Data curation, Formal analysis, Supervision, Writing - review & editing.

Declaration of competing interest

The authors declare that they have no known competing financial interests or personal relationships that could have appeared to influence the work reported in this paper.

Acknowledgment

This research was funded by the NEDO Moonshot Research and Development Program, "C4S Research and Development Project, Calcium Carbonate Circulation System for Construction" (Project manager: Prof. Takafumi Noguchi, The University of Tokyo, Award number: P18016).

Appendix A. Grayscale values by the Auto Threshold type

Table A1. Grayscale values by the Auto Threshold type

	Drip_12h	Drip_24h	RH60	RH85
Default	108	105	102	101
Huang	84	90	85	82
Huang2	86	94	87	83
Intermodes	92	105	100	98
IsoData	108	105	102	101
Li	97	95	90	90
MaxEntropy	202	194	190	194
Mean	115	107	116	121
MinError(I)	64	71	63	64
Minimum	84	81	76	80
Moments	121	125	123	126
Otsu	109	105	102	101
Percentile	119	115	133	139
RenyiEntropy	197	190	188	192
Shanbhag	135	143	136	141
Triangle	72	72	65	63
Yen	204	197	192	199

References

[1] X. Liu, P. Feng, Y. Cai, X. Yu, C. Yu, Q. Ran, Carbonation behavior of calcium silicate hydrate (C-S-H): Its potential for CO_2 capture. Chemical Engineering Journal, 431 (2022), 134243, https://doi.org/10.1016/j.cej.2021.134243.

[2] M. Zajac, J. Skibsted, F. Bullerjahn, J. Skocek, Semi-dry carbonation of recycled concrete paste. Journal of CO2 Utilization, 63 (2022), 102111, https://doi.org/10.1016/j.jcou.2022.102111.

[3] J. Skocek, M. Zajac & M. B. Haha, Carbon Capture and Utilization by mineralization of cement pastes derived from recycled concrete, Scientific Reports, 10 (2020), 5614, https://doi.org/10.1038/s41598-020-62503-z.

[4] M. Zajac, J. Skocek, J. Skibsted, M. Ben Haha, CO_2 mineralization of demolished concrete wastes into a supplementary cementitious material – a new CCU approach for the cement industry, RILEM Tech. Lett. 6 (2021) 53–60, https://doi.org/10.21809/rilemtechlett.2021.141.

[5] S.Y. Pan, T.C. Ling, A.A. Park, P.C. Chiang, An overview: reaction mechanisms and modelling of CO_2 utilization via mineralization. Aerosol Air Qual. Res, 18 (2018), p. 829–848, https://doi.org/10.4209/aaqr.2018.03.0093.

[6] N. Saeki, L. Cheng, R. Kurihara, T. Ohkubo, A. Teramoto, Y. Suda, R. Kitagaki, I. Maruyama, Natural carbonation process in cement paste particles in different relative humidities. Cement and Concrete Composites, 146 (2024), 105400, https://doi.org/10.1016/j.cemconcomp.2023.105400.

[7] S. Steiner, B. Lothenbach, T. Proske, A. Borgschulte, F. Winnefeld, Effect of relative humidity on the carbonation rate of portlandite, calcium silicate hydrates and ettringite. Cement and Concrete Research, 135 (2020), 106116, https://doi.org/10.1016/j.cemconres.2020.106116.

[8] T. R. Marrero, E. A. Mason, Gaseous diffusion coefficients. Journal of Physical and Chemical Reference Data, 1 (1972), 3–118, https://doi.org/10.1063/1.3253094.

[9] F. P. Torgal, S. Miraldo, J. A. Labrincha, J. De Brito, An overview on concrete carbonation in the context of eco-efficient construction: Evaluation, use of SCMs and/or RAC, Construction and Building Materials, 36 (2012), p.141–150, https://doi.org/10.1016/j.conbuildmat.2012.04.066.

[10] E. Drouet, S. Poyet, P. Bescop, J.M. Torrenti, X. Bourbon, Carbonation of hardened cement pastes: Influence of temperature. Cement and Concrete Research, 115 (2019), p. 445–459, https://doi.org/10.1016/j.cemconres.2018.09.019.

[11] Y. Yahui, X. Gang, T. Bin, Carbonation characteristics of cement-based materials under the uniform distribution of pore water, Construction and Building Materials, 275 (2021), 121450, https://doi.org/10.1016/j.conbuildmat.2020.121450.

[12] F.G. Da Silva, P. Helene, P. Castro-Borges, J.B. Liborio, Sources of variations when comparing concrete carbonation results, Journal of Materials in Civil Engineering, 21 (2009), p. 333–342, https://doi.org/10.1061/(ASCE)0899-1561(2009)21:7(333).

[13] V.G. Papadakis, C.G. Vayenas, M.N. Fardis, Fundamental modeling and experimental investigation of concrete carbonation, ACI Mater. J. (1991), p. 363–373.

[14] I. Galan, C. Andrade, M. Castellote, Natural and accelerated CO_2 binding kinetics in cement paste at different relative humidities, Cement and Concrete Research, 49 (2013), p. 21–28, https://doi.org/10.1016/j.cemconres.2013.03.009.

[15] M. Boumaaza, B. Huet, P. Turcry, A. Aït-Mokhtar, The CO_2-binding capacity of synthetic anhydrous and hydrates: Validation of a test method based on the instantaneous reaction rate, Cement and Concrete Research, 135 (2020), 106113, https://doi. org/10.1016/j.cemconres.2020.106113.

[16] Y. Yan, S.-Y. Yang, G.D. Miron, I.E. Collings, E. L'Hôpital, J. Skibsted, F. Winnefeld, K. Scrivener, B. Lothenbach, Effect of alkali hydroxide on calcium silicate hydrate (C-S-H), Cement and Concrete Research, 151 (2022), 106636, https://doi.org/10.1016/j.cemconres.2021.106636.

[17] E.M. Foley, J.J. Kim, M.M. Reda Taha, Synthesis and nano-mechanical characterization of calcium-silicate-hydrate (C-S-H) made with 1.5 CaO/SiO_2 mixture, Cement and Concrete Research, 42 (2012), p. 1225–1232, https://doi.org/10.1016/j.cemconres.2012.05.014.

[18] K. Scrivener, R. Snellings, B. Lothenbach, A Practical Guide to Microstructural Analysis of Cementitious Materials, CRC Press (2015).

[19] H.F.W. Taylor, Cement Chemistry, Thomas Telford Publishing, London, 1990.

[20] D. Snoeck, L.F. Velasco, A.Mignon, S. V. Vlierberghe, P. Dubruel, P. Lodewyckx, N. De Belie, The influence of different drying techniques on the water sorption properties of cement-based materials, Cement and Concrete Research, 64 (2014), p. 54–62, http://dx.doi.org/10.1016/j.cemconres.2014.06.009.

[21] J. Zhang, G.W. Scherer, Comparison of methods for arresting hydration of cement, Cement and Concrete Research, 41 (2011), p. 1024–1036, https://doi.org/10.1016/j.cemconres.2011.06.003.

[22] X. Xu, J. T. Han, D. H. Kim, K. Cho, Two Modes of Transformation of Amorphous Calcium Carbonate Films in Air, The Journal of Physical Chemistry B, 110 (2006), p. 2764–2770, https://doi.org/10.1021/jp055712w

[23] M.P. Asta, A. Fernandez-Martinez, J. Alonso, L. Charlet, N. Findling, V. Magnin, B. Ruta, M. Sprung, F. Westermeier, Nanoscale ion dynamics control on amorphous calcium carbonate crystallization: precise control of calcite crystal sizes, The Journal of Physical Chemistry C, 124 (2020), p. 25645–25656, https://doi.org/10.1021/acs.jpcc.0c08670.

[24] Z. Zhang, Y. Xie, X. Xu, H. Pan, R. Tang, Transformation of amorphous calcium carbonate into aragonite, Journal of Crystal Growth, 343 (2012), p. 62–67, https://doi.org/10.1016/j.jcrysgro.2012.01.025.

[25] F.A. Andersen, L. Brecevic, et al., Infrared spectra of amorphous and crystalline calcium carbonate, Acta Chemica Scandinavica, 45 (1991), p. 1018–1024.

[26] W. Ashraf, J. Olek, Carbonation behavior of hydraulic and non-hydraulic calcium silicates: potential of utilizing low-lime calcium silicates in cement-based materials, Journal of Materials Science, 51 (2016), p. 6173–6191, https://doi.org/10.1007/s10853-016-9909-4.

[27] I. García-Lodeiro, A. Fernández-Jiménez, M.T. Blanco, A. Palomo, FTIR study of the sol–gel synthesis of cementitious gels: C–S–H and N–A–S–H, Journal of Sol-Gel Science and Technology, 45 (2008), p. 63–72, https://doi.org/10.1007/s10971-007-1643-6.

[28] P. Yu, R.J. Kirkpatrick, B. Poe, P.F. McMillan, X. Cong, Structure of calcium silicate hydrate (C-S-H): near-, mid-, and far-infrared spectroscopy, Journal of the American Ceramic Society, 82 (1999), p. 742–748, https://doi.org/10.1111/j.1151-2916.1999.tb01826.x.

[29] E. Kapeluszna, Ł. Kotwica, A. Różycka, Ł. Gołek, Incorporation of Al in C-A-S-H gels with various Ca/Si and Al/Si ratio: microstructural and structural characteristics with DTA/TG, XRD, FTIR and TEM analysis, Construction and Building Materials, 155 (2017), p. 643–653, https://doi.org/10.1016/j.conbuildmat.2017.08.091.

[30] Peter J. McDonald, Ors Istok, Magdalena Janota, Agata M. Gajewicz-Jaromin, David A. Faux, Sorption, anomalous water transport and dynamic porosity in cement paste: A spatially localised 1H NMR relaxation study and a proposed mechanism. Cement and Concrete Research, 133 (2020), 106045, https://doi.org/10.1016/j.cemconres.2020.106045.

[31] V. Shah, K. Scrivener, B. Bhattacharjee, S. Bishnoi, Changes in microstructure characteristics of cement paste on carbonation, Cement and Concrete Research, 109 (2018), p. 184–197, https://doi.org/10.1016/j.cemconres.2018.04.016.

[32] B. Wu, G. Ye, Development of porosity of cement paste blended with supplementary cementitious materials after carbonation, Construction and Building Materials, 145 (2017), p. 52–61, http://dx.doi.org/10.1016/j.conbuildmat.2017.03.176.

[33] B. Šavija, M. Luković, Carbonation of cement paste: understanding, challenges, and opportunities, Construction and Building Materials, 117 (2016) p. 285–301, http://dx.doi.org/10.1016/j.conbuildmat.2016.04.138.

[34] J. J. Chen, J. J. Thomas, H. M. Jennings, Decalcification shrinkage of cement paste, Cement and Concrete Research, 36 (2006), p. 801-809, https://doi.org/10.1016/j.cemconres.2005.11.003.

[35] T.F. Sevelsted, J. Skibsted, Carbonation of C-S–H and C–A–S–H samples studied by 13C, 27Al and 29Si MAS NMR spectroscopy, Cement and Concrete Research, 71 (2015), p. 56–65, https://doi.org/10.1016/j.cemconres.2015.01.019.

[36] M. Castellote, L. Fernandez, C. Andrade, C. Alonso, Chemical changes and phase analysis of OPC pastes carbonated at different CO_2 concentrations, Materials and Structures, 42 (2008), p.515–525, https://doi.org/10.1617/s11527-008-9399-1.

[37] W. Ashraf, J. Olek, Carbonation activated binders from pure calcium silicates: reaction kinetics and performance controlling factors, Cement and Concrete Composites, 93 (2018), p. 85–98, https://doi.org/10.1016/j.cemconcomp.2018.07.004.

[38] C. Kim, J. Kim, S. Joo, Y. Bu, M. Liu, J. Cho, G. Kim, Efficient CO_2 Utilization via a Hybrid Na-CO_2 System Based on CO_2 Dissolution, iScience, 9 (2018), p. 278-285, https://doi.org/10.1016/j.isci.2018.10.027.

[39] S. Ahmad, Reinforcement corrosion in concrete structures, its monitoring and service life prediction—a review, Cement and Concrete Composites, 25 (2003), p. 459–471, https://doi.org/10.1016/S0958-9465(02)00086-0. [41] I. Maruyama, Y. Nishioka, G. Igarashi, K. Matsui, Microstructural and bulk property changes in hardened cement paste during the first drying process, Cement and Concrete Research, 58 (2014), p. 20-34, https://doi.org/10.1016/j.cemconres.2014.01.007.

[42] I. Maruyama, T. Ohkubo, T. Haji, R. Kurihara, Dynamic microstructural evolution of hardened cement paste during first drying monitored by 1H NMR relaxometry, Cement and Concrete Research, 122 (2019), p.107-117, https://doi.org/10.1016/j.cemconres.2019.04.017.

[43] Q.T. Phung, N. Maes, D. Jacques, E. Bruneel, I. Van Driessche, G. Ye, G. De Schutter, Effect of limestone fillers on microstructure and permeability due to carbonation of cement pastes under controlled CO2 pressure conditions, Construction and Building Materials, 82 (2015), p. 376–390, https://doi.org/10.1016/j.conbuildmat.2015.02.093.

[44] L. Li, M. Wu, An overview of utilizing CO_2 for accelerated carbonation treatment in the concrete industry, Journal of CO2 Utilization, 60 (2022), 102000, https://doi.org/10.1016/j.jcou.2022.102000.

[45] L. Li, Q. Liu, V. Dao, M. Wu, Dimensional change of cement paste subjected to carbonation in CO_2 sequestration and utilization context: A critical review on the mechanisms, Journal of CO2 Utilization, 70 (2023), 102444, https://doi.org/10.1016/j.jcou.2023.102444.

[46] D.T. Beruto, R. Botter, Liquid-like H_2O adsorption layers to catalyze the $Ca(OH)_2/CO_2$ solid±gas reaction and to form a non-protective solid product layer at 20°C, Journal of the European Ceramic Society, 20 (2000), p. 497-503, https://doi.org/10.1016/S0955-2219(99)00185-5.

[47] I. Maruyama, W. Kotaka, B. N. Kien, R. Kurihara, M. Kanematsu, H. Hyodo, H. Hirao, R. Kitagaki, M. Tamura, M. Tsujino, S. Fujimoto T. Noguchi, A New Concept of Calcium Carbonate Concrete using Demolished Concrete and CO_2, Journal of Advanced Concrete Technology, 19 (2021), p. 1052-1060, https://doi.org/10.3151/jact.19.1052.